Numerical Investigation of Adjoint Method in Aerodynamic Optimization

M.H. Hekmat and M. Mirzaei
Aerospace Eng. Dep't.
K.N. Toosi Univ. of Tech.

E. Izadpanah
Mech. Eng. Dep't.
Yazd Univ.

ABSTRACT

In this research, the continuous adjoint method is applied to optimize an airfoil in subsonic and transonic flows. An Euler flow solver is used to analyze the inviscid compressible flow over airfoils in each design cycle. Two design problems appearing in aerodynamic shape optimization, namely inverse pressure design and drag minimization were investigated. In the first part, a test case was carried out to evaluate the performance of the adjoint method in inverse design problem. The results show that we can use the adjoint method as an efficient tool in inverse aerodynamic design problems. In the second part, the constrained optimization was investigated in a drag minimization problem. The investigated samples show that a small variation of airfoil geometry has caused considerable decrease in the drag coefficient. To evaluate the performance of the adjoint method in design problems with numerous design variables and also to evaluate the effects of the adoption of the design vector on the optimization results, the constrained drag minimization was performed using two different design vectors. The results shows that the mechanism and the value of drag reduction are affected by the type of design vector. Also, computational cost of the adjoint method are independent of the number of design variables.

Key Words: Adjoint Method, Drag Minimization, Inverse Design, Euler Equations, Design Variables Vector

بررسی عددی روش الحاقی در بهینه سازی آیرودینامیکی

محمد حامد حکمت[1] و مسعود میرزایی[2]
دانشکده مهندسی هوافضا
دانشگاه صنعتی خواجه نصیرالدین طوسی

احسان ایزدپناه[3]
دانشکده مهندسی مکانیک
دانشگاه یزد

(تاریخ دریافت: ۱۳۸۸/۰۲/۲۸، تاریخ پذیرش: ۱۳۸۸/۰۵/۱۴)

چکیده:

در این تحقیق، روش الحاقی پیوسته به منظور بهینه کردن ایرفویل‌ها در جریان‌های مادون صوت و گذر صوت به کارگرفته شده‌است. یک حل کننده جریان به منظور حل میدان جریان تراکم پذیر غیرلزج اطراف ایرفویل در هر سیکل طراحی مورد استفاده قرار گرفت. دو مساله طراحی (که معمولا در بهینه سازی شکل آیرودینامیکی مطرح می شوند)، یعنی طراحی فشار معکوس و کمینه سازی پسا بررسی شده‌اند. در بخش اول، مثالی به منظور ارزیابی عملکرد روش الحاقی در مساله طراحی معکوس اجرا گردید. نتایج نشان می‌دهد که روش الحاقی می‌تواند به عنوان یک ابزار کارآمد در مسائل طراحی معکوس آیرودینامیکی مورد استفاده قرار گیرد. در بخش دوم، بهینه سازی مقید در مساله کمینه سازی پسا مطالعه گردید. مثال‌های بررسی شده نشان می‌دهد که یک تغییر کوچک در هندسه باعث کاهش قابل ملاحظه ای در ضریب پسا می‌شود. به منظور ارزیابی عملکرد روش الحاقی در مسائل با تعداد متغیرهای طراحی زیاد و همچنین به منظور بررسی تاثیر بردار طراحی بر روی نتایج بهینه سازی، کمینه سازی مقید پسا با استفاده از دو بردار طراحی متفاوت انجام گردید. نتایج نشان می دهد که مکانیزم و مقدار کاهش پسا توسط نوع برداری طراحی متاثر می شود. همچنین، هزینه محاسباتی روش الحاقی مستقل از تعداد متغیرهای طراحی است.

واژه های کلیدی: روش الحاقی، کمینه سازی پسا، طراحی معکوس، معادلات اویلر، بردار متغیرهای طراحی

1- Ph.D. Student (Corresponding Author): mhamed_hekmat@yahoo.com
2 - Associate Professor: mirzaei@kntu.ac.ir
3 - Ph.D. Student: izadpanah_ehsan@yahoo.com

1. Introduction

Engineers continually strive to improve their designs, both to increase their operational effectiveness and their market appeal. In the design of a complex engineering system, relatively small design changes can sometimes lead to significant benefits. For example, small changes in wing section shapes can lead to large reduction in shock strength in transonic flow. Changes of this type are unlikely to be discovered by trial and error methods, and for such situations that optimization methods can play an important role.

In the past for a suitable design that provides a desired aerodynamic performance, designers needed to build numerous models for wind tunnel testing to confirm the final design performance. Such a design process does not allow for vast numbers of design iterations or variables to be considered. The development of computational fluid dynamics during recent decades has made possible to evaluate alternative designs by numerical simulation. The use of computational simulation to scan many alternative designs has proved extremely valuable in practice, but it still suffers the limitation finding the best possible design. To ensure the recognition of the true best design, the ultimate goal of computational simulation methods should not just be the analysis of prescribed shapes, but automatic determination of the true optimum shape for the desired application. This is the underlying motivation for the combination of computational fluid dynamics with numerical optimization methods.

The adjoint method is one of a gradient-based method which has been used extensively in many aerodynamic optimization problems in recent decades. Studies of using of the adjoint approach for optimum shape design of systems governed by elliptic equations were initiated by Pironneau [1]. The adjoint equations approach to optimal aerodynamic design was first applied to transonic flow by Jameson [2-4]. He formulated the method for inviscid compressible flows with shock waves governed by both the potential flow and the Euler equations [2]. He implemented the method using surface points as design variables merely and didn't investigate the effect of design variables vector on the results. Elliot and Peraire [5] used the discrete adjoint method on unstructured meshes for the inverse design of airfoils and in transonic flow to produce specified pressure distributions. But they presented merely the complete formulation of the optimal design problem for three dimensions inverse design problem using the adjoint method. Also, they didn't investigate the drag minimization problem and the effect of design variables on the optimization results. In [6], Dadone and Grossman explored the discrete adjoint method and applied it in the progressive optimization strategy. A comparison of both continuous and discrete adjoint approaches was conducted by Nadarajah and Jameson [7-9]. Baysal and Ghayour [10] derived the adjoint equations in Cartesian coordinates on an unstructured grid system using Roe's schemes. Vitturia, and Beuxb [11] implement the discrete adjoint approach for aerodynamic optimization in turbulent viscous flow. The adjoint method has also been used by many researchers in aerodynamic optimization including Xie [12], Qiao [13], Gauger [14], Dwight [15], Amoignon [16] and Hazra [17].

The objective of the present paper is to implement the adjoint approach for airfoils optimization in inverse pressure design and constrained drag minimization problems. First, an inverse design problem is solved to evaluate the optimization algorithm. Second, in the drag minimization problem, the optimization is performed in a fixed lift coefficient and angle of attack is applied as an additional design variable to fix lift during the design process. To evaluate the performance of the adjoint method in design problems with numerous design variables and also to evaluate the effects of the adoption of the design vector on the optimization results, the optimization is performed using two different design vectors. The objective in this study is not merely implementation of the adjoint method. However the objective is implementation and using of adjoint method in order to achieve some results and facts. In fact, we applied adjoint method for inverse design and drag minimization problems and investigated effect design variables vectors on results of the optimization. The result was shown that the mechanism, value and the trend of drag reduction during the optimization process strongly affected by the type of design vector.

2. General Description of the Adjoint Method

For flow over an airfoil or wing, the aerodynamic characteristic defining the cost function (I) are dependent on the flow field variables (w) and the physical location of the boundary, which may be represented as the function F:

$$I = I(w, F). \tag{1}$$

Since w depends on F, a change in F changes the cost function as:

$$\delta I = \left[\frac{\partial I^T}{\partial w}\right]_I \delta w + \left[\frac{\partial I^T}{\partial F}\right]_{II} \delta F \cdot \tag{2}$$

The first term is the contribution of the variation δw in the flow field and the second term is the direct effect of the geometry change. Assume R is the governing equation which expresses the relation of w and F in the flow field domain D, as:

$$R\,(w,F)=0. \tag{3}$$

Then δw is determined, using the equation:

$$\delta R=\left[\frac{\partial R}{\partial w}\right]_I \delta w+\left[\frac{\partial R}{\partial F}\right]_{II} \delta F=0\cdot \tag{4}$$

Since the variation δR is zero, it can be multiplied by a Lagrange Multiplier ψ and subtracted from the variation δI with no change in the result. Thus Eq. (2) can be replaced by:

$$\begin{aligned}\delta I = &\left(\frac{\partial I}{\partial w}\right)^T \delta w+\left(\frac{\partial I}{\partial F}\right)^T \delta F-\psi^T\left(\left[\frac{\partial R}{\partial w}\right]\delta w+\right.\\ &\left.\left[\frac{\partial R}{\partial F}\right]\delta F\right)=\left\{\left(\frac{\partial I}{\partial w}\right)^T-\psi^T\left[\frac{\partial R}{\partial w}\right]\right\}_I \delta w+\\ &\left\{\left(\frac{\partial I}{\partial F}\right)^T-\psi^T\left[\frac{\partial R}{\partial F}\right]\right\}_{II}\delta F.\end{aligned} \tag{5}$$

In order to eliminate the dependency of δI to δw, ψ must satisfy the adjoint equations:

$$\left[\frac{\partial R}{\partial w}\right]^T \psi=\frac{\partial I}{\partial w}\cdot \tag{6}$$

The first term is eliminated and we find that:

$$\delta I=G\,\delta F\ , \tag{7}$$

$$G=\left(\frac{\partial I}{\partial F}\right)^T-\psi^T\left[\frac{\partial R}{\partial F}\right]\cdot \tag{8}$$

According to Eq's. (7) and (8), δI is independent of δw and as a result, for numerous design variables we can compute the gradient vector (G) *with only* one flow solution in addition to one adjoint solution in each design cycle. It should be noted that the computational cost of one adjoint solution is less than one flow solution. After calculating the gradient vector, we can improve the design variables using an optimization algorithm such as steepest descent method or smoothed steepest descent algorithm.

3. Governing Equations

In this study the Euler equations are the governing equations of the field. The conservative form of two-dimensional Euler equations is as:

$$\frac{\partial w}{\partial t}+\frac{\partial f_i}{\partial x_i}=0\quad , \tag{9}$$

where, w is flow variables and f_i is the inviscid flux vector:

$$w=\begin{bmatrix}\rho\\ \rho u_1\\ \rho u_2\\ \rho E\end{bmatrix}\ ,\ f_i=\begin{bmatrix}\rho u_i\\ \rho u_i u_1+\delta_{i1}p\\ \rho u_i u_2+\delta_{i2}p\\ \rho u_i H\end{bmatrix}, \tag{10}$$

and δ_{ij} is the Kronecker delta function and:

$$p=(\gamma-1)\,\rho\left\{E-\frac{1}{2}(u_i^{\,2})\right\}, \tag{11}$$

$$\rho H=\rho E+p\ . \tag{12}$$

In these definitions, ρ, E, H, γ are density, total energy, total enthalpy and heats ratio respectively. Using a transformation from physical coordinates (x_1,x_2) to computational coordinates (ξ_1,ξ_2), the Euler equations can be written as:

$$\frac{\partial W}{\partial t}+R(W)=0\ , \tag{13}$$

$$R(W)=\frac{\partial F_i}{\partial \xi_i},\ W=Jw\ ,\ F_i=S_{ij}f_j\ , \tag{14}$$

$$K_{ij}=\left[\frac{\partial x_i}{\partial \xi_j}\right]\ ,\ J=\det(K)\ ,\ S=JK^{-1}\cdot \tag{15}$$

The scaled contravariant velocity components are introduced as:

$$U_i=S_{ij}u_j\cdot \tag{16}$$

In the computational domain, airfoil surface B_w is represented $\xi_2=0$. The boundary condition on the airfoil surface is:

$$U_2=0\quad On\ B_w\cdot \tag{17}$$

On the far field boundary, the free stream condition is applied.

A finite-volume technique with an artificial dissipation method introduced by Jameson et al. [18], is used to discrete the integral form of the conservation equations. For temporal

approximation, we applied the five stage modified Runge-Kutta approach. Since the time step in explicit methods is small, we applied the convergence acceleration techniques, local time stepping and residual averaging, to accelerate the convergence rate.

4. Adjoint Equations

In this section, we drive the adjoint equations and its boundary conditions for inverse design problem. The design problem can be studied as a control problem choosing airfoil surface as the control function to minimize the cost function I subject to constraints defined by the flow equations. The cost function for inverse design problem is defined as:

$$I=\frac{1}{2}\int_{Bw}(p-p_d)^2\,ds\,, \tag{18}$$

or in the computational domain

$$I=\frac{1}{2}\int_{Bw}(p-p_d)^2\,|ds|d\xi\,, \tag{19}$$

where,

$$|ds|=\sqrt{S_{2j}\,S_{2j}}\,. \tag{20}$$

p_d is the desired pressure on the surface. A variation in the shape results in a variation δI in the cost function:

$$\delta I=\int_{Bw}(p-p_d)\delta p\,ds+\frac{1}{2}\int_{Bw}(p-p_d)^2\,\delta ds\,. \tag{21}$$

From Euler equations in the steady state:

$$\frac{\partial}{\partial\xi_i}\delta F_i=0\,, \tag{22}$$

$$\delta F_i=C_i\,\delta w+\delta S_{ij}\,f_j\,, \tag{23}$$

$$C_i=S_{ij}\,A_j\quad,\quad A_j=\frac{\partial f_j}{\partial w}. \tag{24}$$

Multiplying Eq. (22) by a co-state variable vector, ψ and integrating over the domain, we have:

$$\int_D\psi^T\,\frac{\partial\delta F_i}{\partial\xi_i}\,dD_\xi=0\,. \tag{25}$$

Assuming ψ is differentiable and integrating by parts gives:

$$\int_B n_i\,\psi^T\,\delta F_i\;\;dB_\xi-\int_D\frac{\partial\psi^T}{\partial\xi_i}\delta F_i\;\;dD_\xi=0\,, \tag{26}$$

where, n_i are the components of the unit vector normal to the surface in computational domain. Adding Eq. (26) to the variation of cost function, we have:

$$\delta I=\int_{Bw}(p-p_d)\,\delta p ds+\frac{1}{2}\int_{Bw}(p-p_d)^2\,\delta ds-\int_D\frac{\partial\psi^T}{\partial\xi_i}\delta F_i dD+\int_B(n_i\psi^T\delta F_i)dB\,, \tag{27}$$

where,

$$dD=d\xi\,d\eta\;,\;dB=d\xi\,. \tag{28}$$

From the third integral of Eq. (27), to eliminate the term, which contains δw, the adjoint equations can be obtained:

$$\frac{\partial\psi}{\partial t}-C_i^T\,\frac{\partial\psi}{\partial\xi_i}=0\quad, \tag{29}$$

where, ψ is adjoint variables vector. From flow boundary condition on the surface (Eq. (17)):

$$\delta F_2=\delta p\begin{bmatrix}0\\S_{21}\\S_{22}\\0\end{bmatrix}+p\begin{bmatrix}0\\\delta S_{21}\\\delta S_{22}\\0\end{bmatrix}. \tag{30}$$

The first and fourth integral in Eq. (27) with the above equation follows the adjoint boundary condition on the surface:

$$\psi_2\,n_1+\psi_3\,n_2=p-p_d\,, \tag{31}$$

where, n_1 and n_2 are the components of unit vector normal to the surface:

$$n_j=\frac{S_{2j}}{\sqrt{S_{2j}\,S_{2j}}}. \tag{32}$$

But for better convergence and easier implementation, the adjoint boundary conditions on the surface can be derived as follow [10]:

$$\begin{aligned}
&\psi_{1_{i,1}} = \psi_{1_{i,2}},\\
&\psi_{2_{i,1}} = \psi_{2_{i,2}} + 2n_1(\lambda - n_1\psi_{2_{i,2}} - n_2\psi_{3_{i,2}}),\\
&\psi_{3_{i,1}} = \psi_{3_{i,2}} + 2n_2(\lambda - n_1\psi_{2_{i,2}} - n_2\psi_{3_{i,2}}),\\
&\psi_{4_{i,1}} = \psi_{4_{i,2}},
\end{aligned} \tag{33}$$

where,

$$\lambda = p - p_d. \tag{34}$$

The subscripts (i,1) and (i,2) in the above equations denote cells below and above the wall. On the far field, with attention to fourth integral in Eq. (27), we must choose the ψ such that:

$$n_i \psi^T C_i = 0. \tag{35}$$

For subsonic and transonic flows that the outer boundary is far from the body, we can set:

$$\psi_{1-4} = 0. \tag{36}$$

Because of the similarity of the adjoint equations to flow equations, the same numerical methods used to solve the flow equations can be used to solve the adjoint equations. This greatly simplified the procedure to implement the adjoint module.

If the coordinate transformation is such that $\delta S_{21} and \delta S_{22}$ are negligible in the far field, then the final expression for δI can be written as:

$$\begin{aligned}
\delta I = &\frac{1}{2}\int_{Bw}(p - p_d)^2\,\delta|ds|d\xi -\\
&\int_D \frac{\partial \psi^T}{\partial \xi_i}\delta S_{ij}\, f_j\, d\xi\, d\eta\; -\\
&\int_{Bw}(\delta S_{21}\psi_2 + \delta S_{22}\psi_3)\, p d\xi.
\end{aligned} \tag{37}$$

5. Constrained Optimization

In the drag minimization problem, we want to maintain the lift coefficient constant and equal to its initial value by changing the angle of attack. Therefore, in this case:

$$\delta I = \delta C_d = \frac{\partial C_d}{\partial w}\delta w + \frac{\partial C_d}{\partial F}\delta F + \frac{\partial C_d}{\partial \alpha}\delta\alpha, \tag{38}$$

and the additional constraint is:

$$\delta C_l = \frac{\partial C_l}{\partial w}\delta w + \frac{\partial C_l}{\partial F}\delta F + \frac{\partial C_l}{\partial \alpha}\delta\alpha = 0, \tag{39}$$

or

$$\delta\alpha = -\frac{\frac{\partial C_l}{\partial w}\delta w + \frac{\partial C_l}{\partial F}\delta F}{\frac{\partial C_l}{\partial \alpha}}. \tag{40}$$

The angle of attack is updated using Eq. (40) in each design cycle. To compute $\delta\alpha$ we need to solve an additional adjoint equation. The derivation process of adjoint equations and its boundary conditions for the drag minimization is similar to the inverse design problem. For the drag minimization problem, Eq. (33) can be used to apply adjoint boundary condition. For the drag minimization problem, λ in Eq. (33) is [10]:

$$\begin{aligned}
\lambda = \frac{-2}{\gamma\, p_\infty M_\infty^2\, c}\big[\; &(n_1\cos\alpha + n_2\sin\alpha) +\\
&\Phi(n_2\cos\alpha - n_1\sin\alpha)\;\big]
\end{aligned} \tag{41}$$

$$\Phi = -\frac{\frac{\partial C_d}{\partial \alpha}}{\frac{\partial C_l}{\partial \alpha}}, \tag{42}$$

where, p_∞ and M_∞ are the free stream pressure and Mach number, c is chord length, γ is ratio of specific heats, α is angle of attack and C_l is lift coefficient.

6. Cost Function and Design Variables

The choice of design variables is one of the most crucial steps in any optimization procedure. The success of the optimization of the model problem depends on both the choice of design variables and the cost function.

6. 1 Cost Function

The cost function for the inverse design problem in computational domain is defined as Eq. (19). The cost function for the drag minimization problem in computational domain is defined as:

$$C_d = \frac{-2}{\gamma\, p_\infty M_\infty^2\, c}\int_{Bw} p\,(S_{21}\cos\alpha + S_{22}\sin\alpha)\, d\xi. \tag{43}$$

6. 2 Design Variables

In the present work are utilized two approaches of parameterizing the airfoil. One approach employs the surface mesh points and the other one uses the definition of the NACA 4-digit airfoil series. The use of the surface mesh points as design variables ensures that there is no restriction on the attainable geometry. Since the cost of the adjoint approach is independent of the number of design variables, it is feasible to use the surface points as design variables, whereas the cost would be prohibitive if the gradients were computed by the traditional finite-difference method. In this case, design variables are y components of mesh points on the surface. In NACA 4-digit airfoil series, three parameters, m (the maximum mean camber), p (the chordwise position of the maximum mean camber) and t (maximum thickness of the airfoil) are used to define the airfoil shape. In present work m, t are

taken as design variables and p is assumed to be 0.4.

7. Optimization Algorithm

After calculation of the gradient vector, we can change the design variables using an optimization algorithm. In this work steepest descent algorithm and smoothed steepest descent algorithm has been adapted to treat the design variables towards optimum values. In the steepest descent algorithm, the design variables vector x can be updated as:

$$x^{n+1} - x^n = -\alpha \nabla f \,. \tag{44}$$

where, α is the step length and ∇f is gradient vector of the cost function. It should be noted that the convergence rate of the optimization program is strongly dependent on the step size of α in optimization algorithm. In the smoothed steepest descent algorithm, the design variables vector x can be updated as:

$$\delta x = -\alpha \overline{\nabla} f \,. \tag{45}$$

We replace the gradient ∇f by a smoothed value $\overline{\nabla} f$. To apply smoothing in the x direction, the smoothed gradient $\overline{\nabla} f$ may be calculated using a discrete approximation such as:

$$\overline{\nabla} f - \frac{\partial}{\partial \xi} \varepsilon \frac{\partial}{\partial \xi} \overline{\nabla} f = \nabla f \tag{46}$$

where, ε is the smoothing parameter. The smoothing ensures that each new shape in the optimization process remains smooth. Consequently it is necessary to smooth the gradient vector when we apply surface points as design variables. The smoothing also allows us to use much larger steps, and leads to a large reduction in the number of design iterations. The larger smoothing parameter allows a larger time step to be taken and this leads to accelerate the convergence.

8. Grid Modification

Jameson [2, 4] introduced a grid perturbation method that modifies the current location of the grid points based on perturbations at the surface geometry. The approach is not dependent on the method of structured grid generation. This method was also successfully used by Burgreen et al. [19].

In this method, the grid points are modified along each grid index line projecting from the surface. At first, the arc length between the surface point and the far-field point along the grid line is computed and then the grid points at each location along the grid line are attenuated proportional to its arc length distance from the surface point and the total arc length between the surface and the far-field. The algorithm can be described as:

$$\begin{cases} x_{i,j}^{new} = x_{i,j}^{old} + C_j (x_{i,1}^{new} - x_{i,1}^{old}) \\ \qquad\qquad\qquad\qquad\qquad\qquad j = 2,\ldots,j_{\max} \\ y_{i,j}^{new} = y_{i,j}^{old} + C_j (y_{i,1}^{new} - y_{i,1}^{old}) \end{cases} \tag{47}$$

where, i is the current grid index. The vector C_j can be defined as:

$$C_j = 1 - (3 - 2N_j) N_j^2 \tag{48}$$

where, N_j is the ratio of the arc length from the surface to the current grid point and the total arc length from the surface to the far-field along the grid line that can be written as:

$$N_j = \frac{\sum_{\ell=2}^{j} \sqrt{(x_{i,\ell} - x_{i,\ell-1})^2 + (y_{i,\ell} - y_{i,\ell-1})^2}}{\sum_{\ell=2}^{j_{\max}} \sqrt{(x_{i,\ell} - x_{i,\ell-1})^2 + (y_{i,\ell} - y_{i,\ell-1})^2}}. \tag{49}$$

9. Optimization Results

Finally, the design procedure using the adjoint method can be summarized as Fig. **1**.

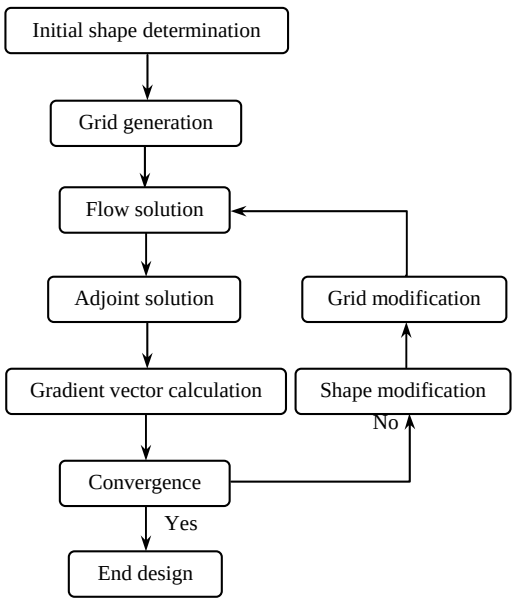

Fig. (1): Design cycle.

9. 1 Inversed Design Problem

In this test case, NACA2415 is designed from NACA4418 airfoil. The flow is subsonic with Mach number of 0.65. Both the initial and target airfoils are at zero degree angle of attack. Airfoil camber (m) and its thickness (t), which are two

parameters in NACA-4digit airfoils definition, are used as the design variables. A 160×80 cells O-Type grid is employed in this calculation. The initial value for *m*, *t* are 0.04, 0.18 and the target value are 0.02, 0.15.

Table **1** presents the design results. The optimal values for *t* and *m* are very close to the target values. It should be noted that convergence of the gradient vector norm was considered as the convergence criteria of the optimization program.

Table (1): Design results.

	Initial	Optimal
m	0.0400	0.02004
t	0.1800	0.15009
I	122E-4	179E-7
$\|G\|$	7.56E-1	3.80E-3

Figure **2** shows the convergence history of the cost function. The convergence rate is very sharp at initial cycles (the main variations of the cost function approximately occur during 20 initial cycles) and after 60 cycles the convergence rate approaches to zero. The final design is obtained after 85 design cycles.

Figure **3** shows the convergence history of the norm of gradient and its components during the design process. In Fig. **3**, the norm of the gradient vector and its components are given simultaneously to show the convergence rate of both the gradient norm and its components. It can be seen that the trend is similar to that of the cost function.

Figure **4** shows variations of the pressure coefficient and the shape during the design process. It can be seen that the pressure distribution approaches to that of the NACA2415.

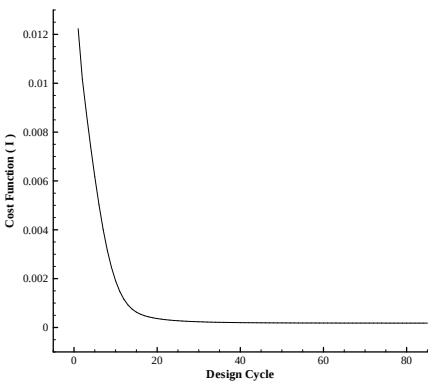

Fig. (2): Convergence histories of the cost function for the inverse design problem.

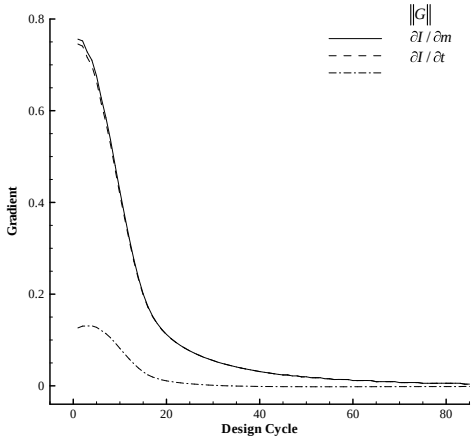

Fig. (3): Convergence history of the norm of the gradient vector and its components for the inverse design problem.

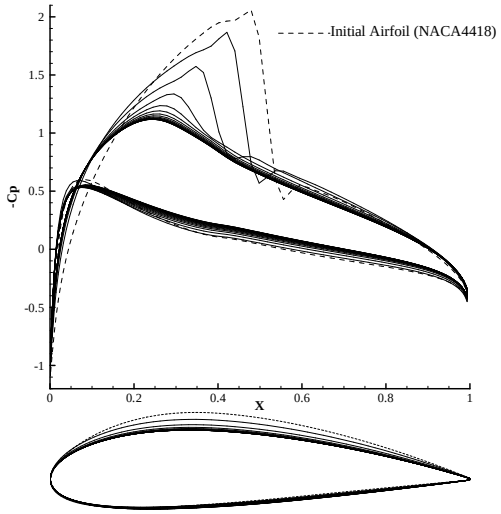

Fig. (4): Variations of pressure distribution and airfoil shape in the inverse design problem.

To validate the adjoint code, the gradients of the adjoint method were compared with those of the finite difference method. Table **2** compares results of adjoint method and the finite difference method. It can be seen that a very good conformity of the finite difference and adjoint gradients.

Table (2): Comparison of the adjoint and the finite difference methods.

	$\partial I / \partial m$	$\partial I / \partial t$
Adjoint Method	0.7454	0.1263
Finite Difference Method	0.7446	0.1259

9. 2 Drag Minimization Problem

In this case, we have implemented the method in the constrained drag minimization. To evaluate the performance of the adjoint method in design problems with numerous design variables and also to evaluate the effects of the adoption of the design vector on the optimization results, the constrained drag minimization is performed using two different design vectors. In first test case, the surface points are used as the design variables and in the second test case, *m* and *t* are adopted as design variables. The design is started by a NACA0012 airfoil at 3.0 degrees angle of attack. The flow is transonic with Mach number of 0.75. We performed computations on a 160×80 O-grid.

A. the optimization using the surface points (Test Case I)

Table **3** represents the design results. The reduction in the drag coefficient is considerable. We obtained 80.7 percents reduction in drag coefficient but lift coefficient variations is very small (1.4 percents).

Table (3): Design results.

	Initial	Optimal
C_d	0.0317	0.0062
C_l	0.6027	0.5937
α	3	1.17

Figure **5** represents the convergence of the cost function. This figure shows that full convergence of aerodynamic optimization is obtained after 260 design iterations. 49.65 percents reduction in drag coefficient is attained after 30 design cycles. Only 1.74 percents drag reduction is obtained during 120 final cycles. Figure **6** shows the convergence history of the norm of gradient during the design process. According to this figure the trend is similar to that of the cost function variations.

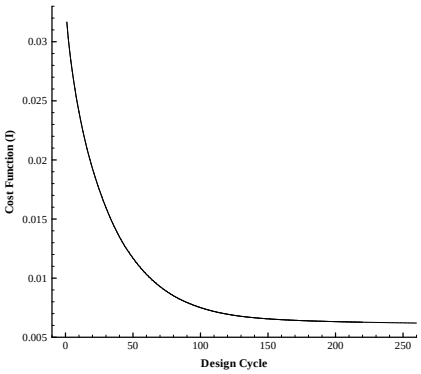

Fig. (5): Convergence histories of the cost function for the drag minimization problem.

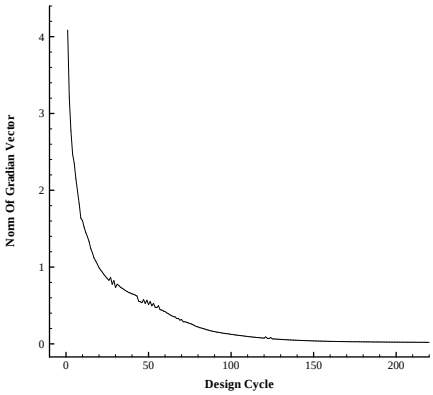

Fig. (6): Convergence history of the norm of the gradient vector for the drag minimization problem.

Figure **7** shows the geometry of initial and optimal airfoils. The change in the upper surface and around the trailing edge is considerable, whereas the change in the lower surface is very small. Figure **8** compares the initial and optimal pressure contours. Figure **9** represents the initial and optimal pressure coefficients. The figure shows that the strong shock on the initial airfoil surface has been strongly weakened and consequently the drag coefficient has been reduced but the surface area under the curve which is represented the value of the lift coefficient has been remained constant and consequently this coefficient is nearly the same for both the initial and optimal airfoils. Figures **7** and **9** show that the upper surface of the optimal airfoil has approached to a flat geometry. The flat surface has weakened the strength of the shock wave. Further more the geometry of the airfoil at the trailing edge has curved downward to compensate the reduction of the lift coefficient due to weakening the strength of the shock. It should be noted that for propose of fixing the lift coefficient, the angle of attack is considered as an extra design variable.

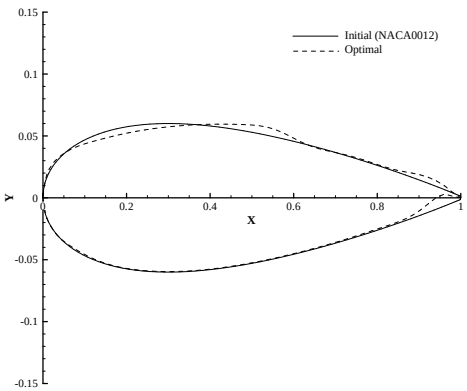

Fig. (7): Comparison of NACA0012 airfoil and optimal airfoil for the drag minimization problem.

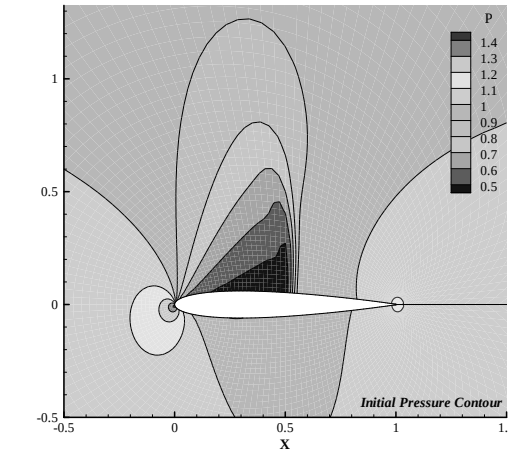

(a)

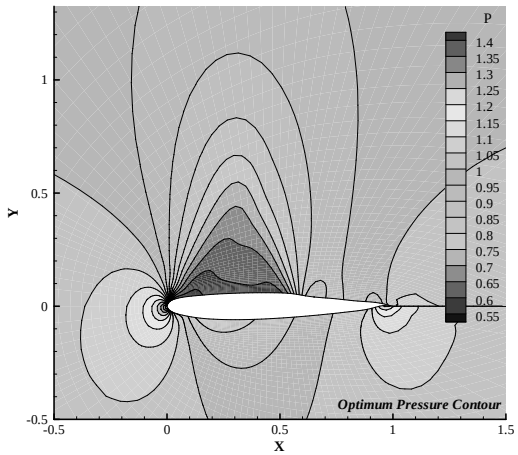

(b)

Fig. (8): Pressure distribution contours for the drag minimization problem. (a) Initial and (b) optimal

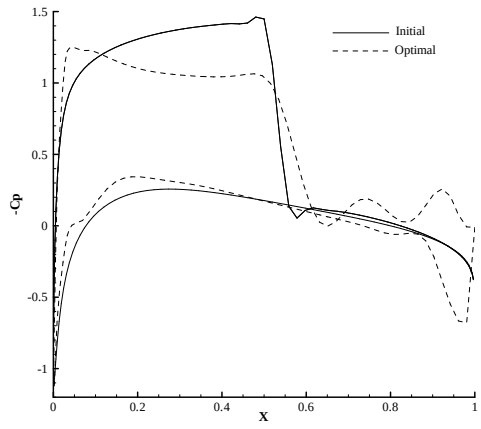

Fig. (9): Comparison of pressure coefficient of NACA0012 and optimal airfoils for the drag minimization problem.

B. the optimization using the relations of the NACA 4-digit airfoil series (Test Case II)

Table **4** represents the design results. The reduction in the drag coefficient is considerable. We obtained 83.28 percents reduction in drag coefficient but lift coefficient variations is very small (0.4 percents).

Table (4): Design results.

	Initial	Optimal
m	0.00	0.01072
t	0.12	0.0501
C_d	0.0317	0.0053
C_l	0.6027	0.6003
α	3	2.24

Figure **10** gives the variation of the cost function with design cycle. For this problem, the design cycle has 170 iterations. The drag coefficient reduction is 81.92 percents during the first 80 design cycles. This coefficient has only 1.36 percents reduction the last 90 cycles.

Figure **11** shows the variation of the norm of the gradient vector with design cycle. The trend is similar to that of the cost function. Regarding to Fig's. **10-11** the convergence of the optimization program is evident.

Figure **12** gives the pressure coefficients on upper and lower surface of initial and optimal airfoils. It is seen that the location of the shock wave has changed and its strength is reduced. But the surface under the curve is remained constant which reveals no change in lift coefficient. It is clear that the drag coefficient reduction has been achieved due to reduction of thickness, whereas increase of the camber has led to increase the lift coefficient. In fact the reduction of the lift due to the reduction of the thickness has been compensated by increase of the camber. More over the variation of the angle of attack is such that the lift coefficient remains constant.

Figure **13** shows the pressure contours around the initial and optimal airfoils. Regarding to this figure, the shock wave has moved toward the leading edge and its strength is considerably reduced.

It should be noted that the convergence rate of the optimization program is strongly dependent on the step size of α in optimization algorithm. If the step size was taken larger, it increased the convergence rate. But adoption of a larger step size for α leads to increase in geometry parameters (design variables) and decrease in accuracy of the

calculated gradients. Sometimes larger step size caused oscillatory behavior of the gradients. More over adoption of smaller step size for α led to increase in number of design cycles.

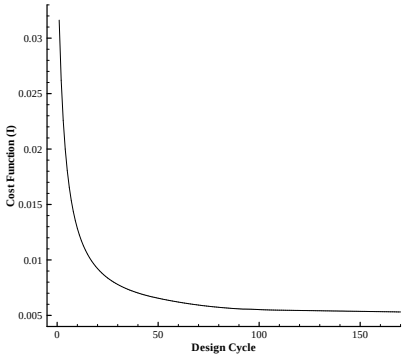

Fig. (10): Convergence history of the cost function for the drag minimization problem.

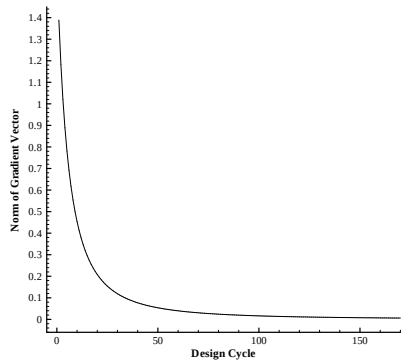

Fig. (11): Convergence history of the norm of the gradient for the drag minimization problem.

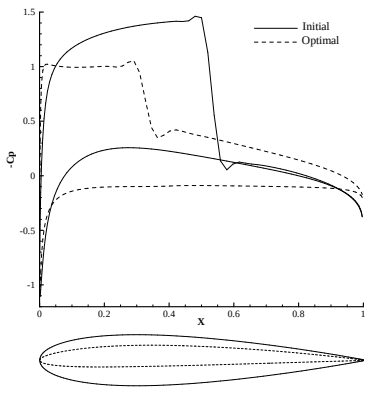

Fig. (12): Comparison of pressure coefficient and geometry of NACA0012 and optimal airfoils for the drag minimization problem.

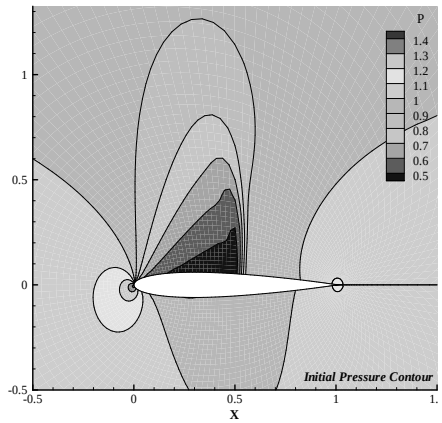

(a)

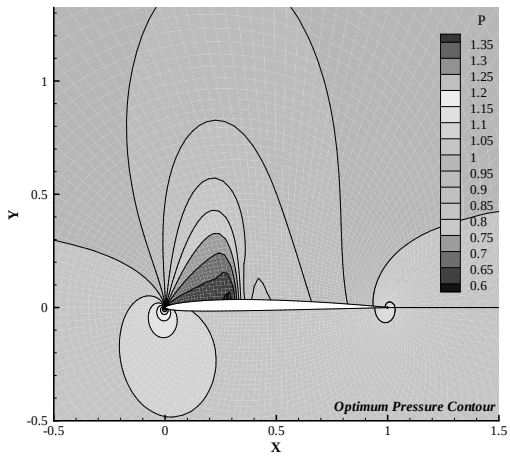

(b)

Fig. (13): Pressure distribution contours for the drag minimization problem. (a) Initial and (b) optimal.

It is known that the location and strength of a shock wave in transonic regime is a main parameter in drag calculation. Comparison of results of the optimization problem using two different design vectors, in on of them the surface points are considered as design variables and in the other one, the parameters of four digit NACA airfoil are design variables (Fig's. **8** and **13** or Fig's. **9** and **12**), shows that when the surface points of the airfoil are design variables the upper surface geometry changes such that the strength of the shock wave is reduced but the location of the shock wave has no change, in fact the drag reduction is carried out via the variation of the curvature only at region of the shock wave. And the lift coefficient is recovered via the increase in curvature only at the trailing edge region. When the thickness and camber of NACA four digits were considered as design variables, the shock wave moves toward the leading edge and the strength is reduced. In fact the drag

reduction is carried out via reduction of the thickness on all of the surface points and recovery of the lift coefficient is achieved with increasing the camber on all of the surface points.

Table **5** summarizes the required runtime and number of adjoint and flow solvers to achieve the convergence of the optimization program for the constrained drag minimization problem. The used computer specification is "Intel(R) Core(TM) Due CPU T2450@ 2.00GHz, 1GB of RAM".

Table (5) Runtime and number of adjoint and flow solvers of the drag minimization problem.

	Test Case I	Test Case II
Runtime	504 minutes	425minutes
Number of Adjoint Solvers	440	340
Number of Flow Solvers	220	170
Number of Design Cycles	220	170

10. Conclusion

In this paper, we implemented the adjoint method for the inverse pressure design and the constrained drag minimization problems. In the inverse design problem, values of camber and thickness (design variables) were obtained successfully. The results of the test case show that we can use the adjoint approach as an efficient tool in airfoil inverse design problem. To evaluate the performance of the adjoint method in design problems with numerous design variables and also to evaluate the effects of the adoption of the design vector on the optimization results, the minimization was performed using two different design vectors. It was shown that the mechanism and the trend of drag reduction during the optimization process strongly affected by the type of design vector. By using this method, we can design high lift or low drag airfoils according to the desired surface pressure.

11. References

1. Pironneau, O., "Optimal Shape Design for Elliptic Systems", Springer-Verlag, New York, 1984.
2. Jameson, A., "Aerodynamic Design via Control Theory", J. Scientific Computing, Vol. 3, No. 4, pp. 233-260, 1988.
3. Jameson, A. and Alonso, J., "Automatic Aerodynamic Optimization on Distributed Memory Architectures", AIAA Paper 96-0409, The 34th Aerospace Sciences Meeting and Exhibit, Reno, Nevada, 1996.
4. Jameson, A., "Re-engineering the Design Process through Computation", AIAA Paper 97-0641, The 35th Aerospace Sciences Meeting and Exhibit, Reno, Nevada, 1997.
5. Elliott, J. and Peraire, J., "3-D Aerodynamic Optimization on Unstructured Meshes with Viscous Effects", AIAA Paper 97-1849, The 35th Aerospace Sciences Meeting and Exhibit, Reno, Nevada, 1997.
6. Dadone, A. and Grossman, B., "Progressive Optimization of Inverse Fluid Dynamic Design Problems", J. Comp. & Fluids, Vol. 29, No. 2, pp. 1-32, 2000.
7. Nadarajah, S. and Jameson, A., "A Comparison of the Continuous and Discrete Adjoint Approach to Automatic Aerodynamic Optimization", AIAA Paper 2000-0667, The 38th Aerospace Sciences Meeting and Exhibit, Reno, Nevada, 2000.
8. Nadarajah, S. and Jameson, A., "Studies of the Continuous and Discrete Adjoint Approaches to Viscous Automatic Aerodynamic Shape Optimization", AIAA Paper 2001-2530, The 15th. Comp. Fluid Dyn. Conf., Anaheim, 2001.
9. Nadarajah, S., "The Discrete Adjoint Approach to Aerodynamic Shape Optimization", Ph.D. Dissertation, Mech. & Aerospace Eng. Dep't., Stanford Univ., Stanford, USA, 2003.
10. Xie, L., "Gradient-based Optimum Aerodynamic Design, Using Adjoint Methods", Ph.D. Dissertation, Virginia Polytechnic Institute and State Univ., Virginia, USA, 2002.
11. Baysal, O. and Ghayour, K. "Continuous Adjoint Sensitivities for Optimization with General Cost Functional on Unstructured Meshes", J. AIAA, Vol. 39, No. 1, pp. 48-55, 2001.
12. Michieli-Vitturia, M. and Beuxb, M.F., "A Discrete Gradient-based Approach for Aerodynamic Shape Optimization in Turbulent Viscous Flow", J. Finite Elements in Analysis and Design**,** Vol. 5, No. 12, pp. 187-202, 2006.
13. Qiao, Z.D., Yang, X.D., Qin, X.L., and Zhu, B., "Numerical Optimization Design by Solving Adjoint Equations", ICAS Cong., 2002.
14. Gauger, N.R. and Brezillon, J., "Aerodynamic Shape Optimization, Using Adjoint Method", J. Aero. Soc. of India, Vol. 54, No. 3, pp. 110-121, 2002.
15. Dwight, R.P. and Brezillon, J., "Effect of Various Approximations of the Discrete Adjoint on Gradient-based Optimization", The

44th AIAA Aerospace Sciences Meeting and Exhibit, Reno Nevada, 2006.
16. Amoignon, O., "Adjoint-based Aerodynamic Shape Optimization", Ph.D. Dissertation, Mech. Eng. Dep't., Uppsala Univ., Sweden, 2004.
17. Hazra, S.B., "An Efficient Method for Aerodynamic Shape Optimization", The 10th AIAA/ISSMO Multidisciplinary Analysis and Optimization Conf., New York, USA, 2004.
18. Jameson, A., Schmidt, W., and Turkel, E., "Numerical Solutions of the Euler Equations by Finite Volume Methods with Runge-Kutta Time Stepping Schemes", AIAA Paper 81-1259, 1981.
19. Burgreen, G.W. and Baysal, O., "3-D Aerodynamic Shape Optimization of Wings, Using Sensitivity Analysis" AIAA Paper 94-0094, The 32nd Aerospace Sciences Meeting and Exhibit, Reno, Nevada, 1994.